A high-resolution simulation of the ocean during the POMME experiment: Mesoscale variability and near surface processes

A. Paci,[1] G. Caniaux,[1] H. Giordani,[1] M. Lévy,[2] L. Prieur,[3] and G. Reverdin[2]

Received 13 November 2005; revised 30 October 2006; accepted 26 December 2006; published 10 April 2007.

[1] This article is the second part of a modeling study of upper ocean mesoscale physical processes in an area of the northeast Atlantic that was extensively sampled during the Programme Océan Multidisciplinaire Méso-Echelle (POMME experiment, October 2000–September 2001). The model is a high-resolution regional version of the ocean general circulation model OPA integrated from February to May 2001. The mesoscale upper ocean dynamics has been carefully validated in a first paper (Paci et al., 2005). In the present article, the simulation is used to analyze the contribution of mesoscale eddies to the mixed layer processes during the period that controls the annual subduction rate and the characteristics of the subducted water. Mesoscale eddies account for a significant part of the mixed layer heat, salt, and water budgets through mesoscale and submesoscale structures acting on the horizontal advective terms. They represent respectively 52% and 66% of the horizontal advection of temperature and salinity and 70% of the lateral induction. They also induce an earlier and more intense restratification. The domain-averaged detrainment appears to be reduced by more than 15% by mesoscale eddies and reaches about 0.8 Sv. However, these eddies increase the density of the detrained water. Some dense water, likely to be involved in the formation of subpolar mode water, is detrained by them in a way that maximizes its chance to be effectively subducted in the area.

Citation: Paci, A., G. Caniaux, H. Giordani, M. Lévy, L. Prieur, and G. Reverdin (2007), A high-resolution simulation of the ocean during the POMME experiment: Mesoscale variability and near surface processes, *J. Geophys. Res.*, *112*, C04007, doi:10.1029/2005JC003389.

1. Introduction

[2] Oceanic subduction is the process by which water enters into the permanent pycnocline and leaves definitely the mixed layer over the course of a year. In the subtropical gyres, these subducted water are involved in the renewal of the thermocline water masses and remain isolated on a decadal timescale from the influence of the atmosphere [*Thiele and Sarmiento*, 1990]. Then a good knowledge of their subduction mechanism and the processes associated are required to understand the interannual to interdecadal climate variability. Subduction has been first interpreted as the results of Ekman pumping and horizontal advection by the mean current across the mixed layer base [e.g., *Marshall et al.*, 1993]. Later, *Marshall* [1997] shows that this approach is not appropriate for regions of intense baroclinic instability. If the role of mesoscale eddies is now recognized in regions of intense eddy activity [e.g., *Hazeleger and Drijfhout*, 2000; *Qu et al.*, 2002], their effect is often supposed nonsignificant in less active regions. However, there is growing evidence, both from in situ data [*Weller et al.*, 2004] and from numerical studies [*Valdivieso Da Costa et al.*, 2005; *Gebbie*, 2007] that they may have a significant impact on subduction, even in these regions.

[3] The Programme Océan Multidisciplinaire Méso-Echelle (POMME) provides an exceptional framework to study this question. POMME has indeed been designed to study the subduction of a particular water mass, called mode water because of its vertical homogeneity, and the associated biogeochemical processes in a particular area of the northeast Atlantic [*Mémery et al.*, 2005; *Reverdin et al.*, 2005]. This relatively quiescent region is located halfway between the Azores and the Iberian Peninsula. Subduction in this area has been explained in terms of advection of subpolar mode water to the south by the southern branches of the North Atlantic current across a steep mixed layer depth gradient [e.g., *Paillet and Arhan*, 1996a, 1996b]. Beside this large-scale view, implicitly neglecting mesoscale eddies, POMME focuses precisely on their role, not only in the subduction mechanisms of 11–13°C mode water, but also in biological production and in the carbon budget of the northeast Atlantic. Indeed, this area is also a strong sink of atmospheric CO_2 [*Takahashi et al.*, 1995]. The POMME domain, a 500-km longitude by 750-km latitude area centered on 41.5°N/18.3°W (see Figure 1), has been investigated from the fall 2000 to the fall 2001.

[1] Centre National de Recherches Météorologiques-Groupe d'Etude de l'Atmosphère Météorologique, Météo-France/CNRS, Toulouse, France.
[2] LOCEAN/IPSL, University of Paris VI, Paris, France.
[3] LOV, Villefranche-sur-Mer Cedex, France.

0148-0227/07/2005JC003389

[4] The present article focuses on the February to May 2001 period, described by the two intensive hydrographic surveys POMME 1 and POMME 2 (hereafter P1 and P2). P1 was aimed at describing the late winter conditions, in particular the mixed layer depth field and the prebloom distribution of physical and biogeochemical data. Fifty days later, the cruise P2 followed P1 in order to describe the restratification and the spring bloom. Each cruise was divided in two legs (hereafter L1 and L2). The first legs were dedicated to a large-scale survey of the area, whereas the second legs focused on some specific mesoscale structures. Because of its importance, this period has been particularly well described, and an impressive amount of data have been collected during the field experiments. However, data are isolated in time and space and need to be integrated into three-dimensional fields permitting a realistic spatiotemporal representation of the processes occurring in the upper ocean. Two 1-year numerical studies have been conducted by *Gaillard et al.* [2005] (using a simplified Kalman filter) and by *Giordani et al.* [2005a, 2005b] (using a simplified primitive equation model) in order to meet these objectives. But the simplifications carried on these models somehow limit their use for realistic mesoscale process studies.

[5] In a first paper [*Paci et al.*, 2005], the results of a high-resolution oceanic model using measured data have been presented and validated through comparisons with a wide range of in situ and satellite observations. The implementation of the full primitive equation avoids the drawbacks found in the other numerical studies of the POMME area. The model has also been successfully coupled with a biological model to study biogeochemical processes [*Lévy et al.*, 2005]. A second simulation, without mesoscale eddies, is used in the present article as a reference to be compared with this simulation in order to assess their effects. Our aim is not to conduct a study of the subduction in itself, which would require at least a 1-year simulation, and probably on a larger area. But it is to analyze the contribution of mesoscale eddies to the processes associated with subduction during a period that controls the annual subduction rate and the characteristics of the subducted water.

[6] Section 2 presents the numerical model and the two numerical simulations (with and without mesoscale eddies). The simulations are used to study the effect of mesoscale eddies in the evolution of the mixed layer temperature (section 3) and salinity (section 4), as well as in the water mass exchange with the pycnocline (section 5). Finally, the main results of this study are summarized in section 6.

2. The Simulations

[7] This section presents the numerical model and the two numerical simulations (mesoscale and nonmesoscale). They will be used later on to study the effect of mesoscale eddies on the processes occurring in the mixed layer during the late Winter and Spring of 2001 in the POMME area.

2.1. Regional Ocean Model

[8] The three-dimensional model used in this study is derived from the ocean general circulation model OPA developed at the Laboratoire d'Océanographie Dynamique et de Climatologie (LODYC) and described in detail by *Madec et al.* [1999] (available at http://www.ipsl.jussieu.fr). The regional version was first set up by *Caniaux et al.* [1993]. The present version includes a surrounding recirculation area separated from the physical domain (the interior) by a buffer zone in which T and S fields are damped [*Gavart et al.*, 1999].

[9] The model domain is a 500-km longitude by 750-km latitude area, extending from 15.33°W to 21.33°W and from 38°N to 45°N, which is the POMME area where the four hydrological surveys were performed (POMME 0, POMME 1, POMME 2, and POMME 3). The horizontal regular grid spacing is 1/20° (about 5 km), therefore there are 121×141 horizontal grid points. The vertical grid, using prescribed z-levels, has 69 levels down to 5650 m with 5-m-thick layers in the first 100 m; the thickness then gradually increasing downward to the bottom. The lower boundary is a high-resolution bathymetry provided by the Hydrographic Service of the French Navy (SHOM) (see Figure 1). The upper boundary is flat (rigid-lid approximation) and is forced by daily air–sea fluxes.

[10] These fluxes have been computed from in situ data, satellite data, and ECMWF weather prediction model outputs with specific state-of-the-art bulk formulae [*Caniaux et al.*, 2005a]. Then observed mixed layer heat and salt budgets have been used to adjust the fluxes [*Caniaux et al.*, 2005b]. The damping fields used at the lateral boundaries are computed from the P1L1 hydrographic survey (3–23 February 2001, Figure 2) and from the P2L1 hydrographic survey (24 March to 12 April 2001, Figure 2). Figure 2 shows also many cyclonic (C2, C4, C5, C6, and C7) and anticyclonic (A1, A2, A4, A5, and A7) eddies observed during P1 and P2, which were more numerous than what was expected in this region according to *Paillet* [1999]. The exhaustive mesoscale eddy nomenclature of the POMME domain is presented in *Mémery et al.* [2005].

2.2. The Mesoscale Simulation

[11] In this simulation, the initial mass and the current fields have been deduced from the P1L1 hydrographic survey (Figure 2). The model has been integrated from 13 February to 20 May 2001 without using any other data assimilation than the air–sea fluxes and lateral boundaries. Indeed, the air–sea fluxes used provide a way to assimilate the observed SST, as well as the observed mixed layer heat and salt budgets. The lateral boundary condition used provide also a way to assimilate the characteristics of the entering water owing to the P1L1 and P2L2 hydrographic survey data. In order to be able to realize a valuable process study, it was particularly important not to use an assimilation technique inconsistent with the physics and thermodynamics of the model. The success of our approach is also partly due to the fact that the circulation is dominated by a few slow evolving mesoscale eddies. These main mesoscale eddies are not formed in the area [*Le Cann et al.*, 2005], but they are embedded in the initial mass and current fields.

[12] The simulation results have been carefully validated through comparisons with the extensive data set collected during P1 and P2 [*Paci et al.*, 2005]. The simulation reproduces properly the large-scale gradients in the area as well as the mesoscale features (position and intensity), according to the comparisons with data from thermosalinograph (TSG), conductivity–temperature–depth (CTD), and vessel-

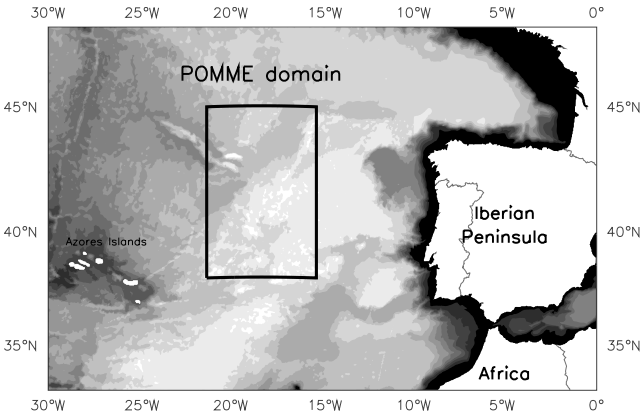

Figure 1. Map of the experiment and simulation domain. Bathymetry is represented by 12 grey tone-filled isobaths evenly spaced from 5500 m depth to the surface, the lighter tone corresponding to depths greater than 5500 m (figure reproduced from *Paci et al.* [2005]).

mounted acoustic Doppler current profiler (VM-ADCP). Not only the upper ocean dynamics has been validated but also the deep ocean dynamics by quantifying the baroclinic horizontal mass transports, integrating water properties from 20 to 1670 m. The comparison between baroclinic horizontal transports from the model fields and from the analysis of the hydrological survey at P2L1 demonstrates that the water mass properties of the 20- to 1670-m layer are correct.

[13] Simulated MLD has been compared favorably with the MLD deduced from the CTD measurements. In particular, the variability is of the same order of magnitude in the CTD- and model-computed MLD, which is an important point indicating that the small MLD structures seen in Figure 3 are not likely to be numerical artifacts.

[14] Vertical velocity is a very difficult field to measure and to interpret, one reason being its dependence on the scale at which it is measured. Few direct measurements of oceanic vertical velocities have been done, and most of them in deep convection area where intense vertical velocities are found [e.g., *Lherminier et al.*, 1999; *Lavender et al.*, 2002; *Steffen and D'Asaro*, 2002]. Their interpretation is not an easy task and may even necessitate some complementary data, for example, the results of a numerical simulation [*Lherminier et al.*, 2001]. Some RAFOS-VCM floats have been deployed during the POMME experiment, but interpretation of the available data is still under consideration. Therefore it has not been possible to compare the simulated vertical velocity with direct measures of the vertical velocity. However, very similar small-scale structures were observed in the same simulation but with a resolution of 2.5 km according to a test reported by *Lévy et al.* [2005] and in a different three dimensional numerical model simulation [*Giordani et al.*, 2005a, 2005b]. Even if these arguments do not originate from observations, they provide evidence for the vertical velocity fields simulated. Moreover, the overall shape and intensity of the simulated vertical velocities is consistent with the preliminary results of indirect estimates from in situ measurements using the method presented in *Giordani et al.* [2006], as well as with the indirect estimates from in situ measurements of *Legal et al.* [2007].

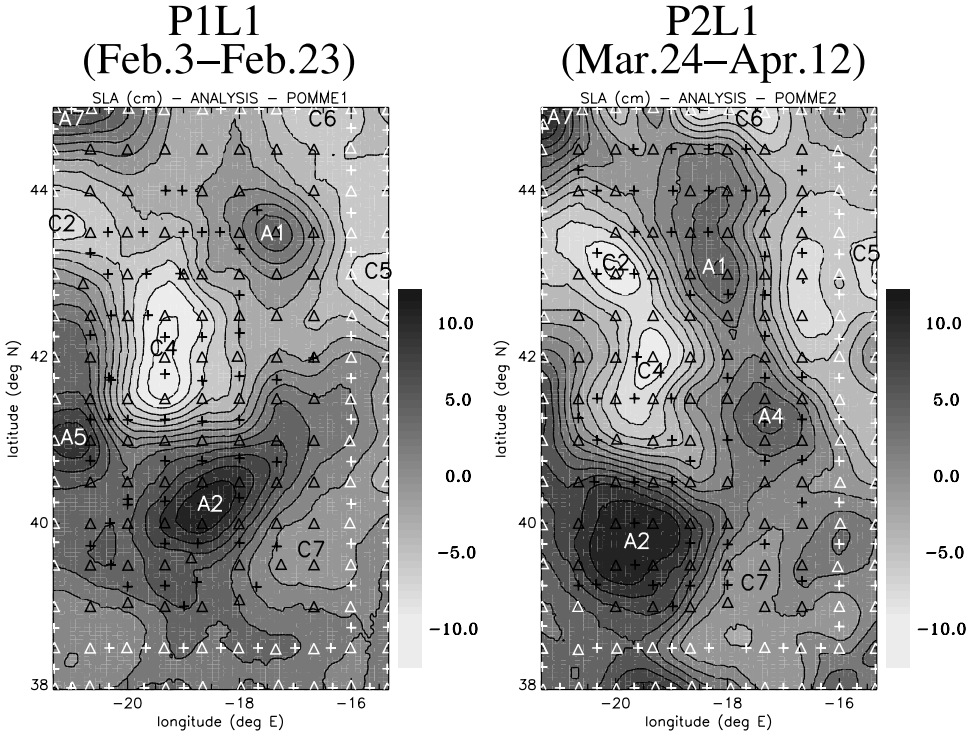

Figure 2. Hydrological surveys performed during the first leg of POMME 1 and POMME 2, with the conductivity–temperature–depth (CTD) shots by the R/V *L'Atalante* (black triangles) and R/V *D'Entrecasteaux* (white triangles), expandable bathythermograph (XBT) shots by the R/V *L'Atalante* (black crosses) and R/V *D'Entrecasteaux* (white crosses), and sea level anomalies (SLA) estimated from the objective analyses performed on these data sets.

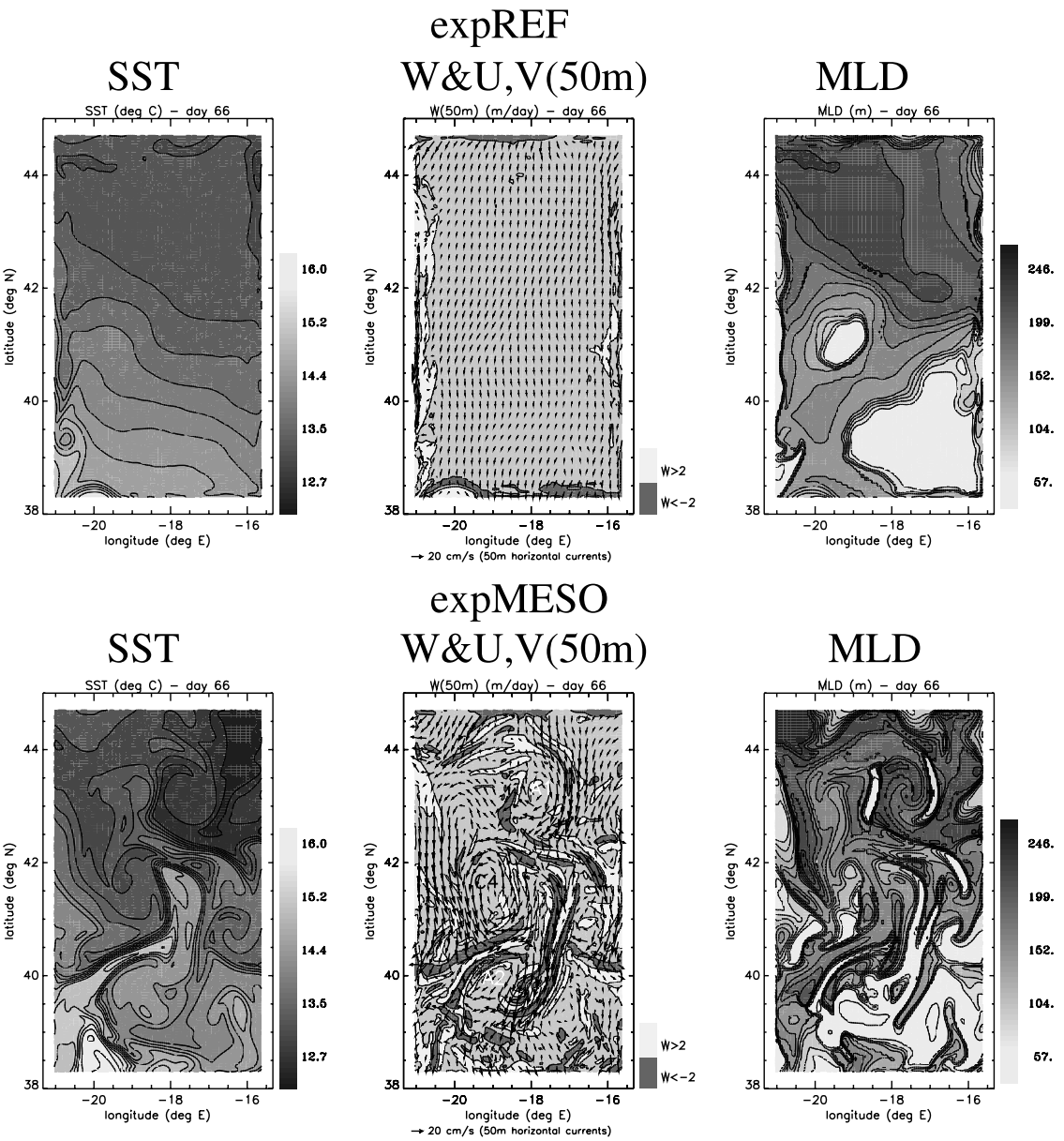

Figure 3. One-day averaged sea surface temperature, vertical and horizontal velocities at 50 m depth, and mixed layer depth on 7 March 2001 (during the mixed layer shallowing) for expREF (first line) and for expMESO (second line). An effect of the mesoscale eddies seen on temperature and horizontal velocity fields in expMESO is to produce some intense mixed layer and vertical velocities submesoscale structures.

[15] Table 1 summarizes the simulation validations conducted. Finally, the model captures realistically both the upper ocean features and the baroclinic transport in the 20- to 1670-m layer. The model has successfully integrated isolated data into three-dimensional realistic fields. The full mesoscale dynamics of the POMME area at this period is represented in this simulation, which will be referred to as expMESO.

2.3. The Nonmesoscale Simulation

[16] In this simulation, the initial mass and the current fields have been deduced from a mesoscale-filtered P1L1 analysis. The mesoscale has been removed from the P1L1 analysis by averaging it in strips perpendicular to the mean large-scale density gradient. In order to have the same characteristics of the entering water than in expMESO, the structures close to the lateral boundaries have been kept by progressively merging the mesoscale-filtered field with the original field close to the lateral boundaries. This is the only difference with expMESO. As there is no input of energy in the model other than through air–sea fluxes and lateral boundaries, and because the main mesoscale eddies were not formed in the area, it has been sufficient to remove the mesoscale to the initial state in order to damp the mesoscale activity over the whole simulation. On average over the duration of the experiment, the eddy kinetic energy from

Table 1. Correlations Between Model and Data Fields From P1L1 to P2L2 for the run expMESO Used in This Article[a]

Correlation model/data fields	(1) SST	(2) SSS	(3) T (200 m)	(4) S (200 m)	(5) (U,V)	(6) Transport
expMESO	0.92	0.87	0.89	0.88	0.70	0.80

[a](1) and (2) SST and SSS from TSG; (3) and (4) T (200 m) and S (200 m) from CTD; (5) VM-ADCP horizontal currents in the 60- to 460-m layer; (6) baroclinic horizontal transport anomalies (relative to the P1L1 hydrological survey) in the 20- to 1670-m layer from the P2L1 hydrological survey (table reproduced from *Paci et al.* [2005]).

100 to 1670 m has been reduced by more than 85% compared to expMESO. This nonmesoscale simulation will be referred to as expREF. It will be used as a reference to be compared with expMESO in order to assess the effect of mesoscale eddies. It is important to note that the same air–sea fluxes are used in both experiments. Therefore the differences between expMESO and expREF will result only from the oceanic mesoscale dynamics, and not from the impact of oceanic mesoscale eddies on air–sea fluxes. However, these fluxes do contain a mesoscale signal linked to the mesoscale eddies present during the POMME experiment.

2.4. Some Results

[17] Both simulations, lasting from 13 February to 20 May 2001, are characterized by a warming of upper ocean waters and a restratification of the mixed layer, in response to positive net surface heat fluxes associated with rather weak winds [*Paci et al.*, 2005]. Besides this domain-scale evolution, there is a strong deformation of the temperature and salinity fields by advection and stirring induced by mesoscale eddies in expMESO (Figure 3).

[18] The results show also a strong impact of mesoscale eddies on mixed layer depth and vertical velocity fields. Actually one of the most striking differences between expMESO and expREF is the development of filament-shaped vertical velocity structures in expMESO, in particular during the restratification of the mixed layer, as shown in *Paci et al.* [2005]. These structures are localized at the periphery of the eddies (see Figure 3), where the deformation (or the mixed layer horizontal gradient) induced by the eddies is important [*Giordani et al.*, 2006]. Some of these structures may persist for a few days. The typical width of these filaments localized in the upper few hundred meters is 10–20 km. Their averaged intensity is a few meters per day, but vertical velocities larger than 25 m day^{-1} are found at some locations, the highest values being obtained during the restratification period.

[19] Another interesting difference between expMESO and expREF is the mixed layer depth field (hereafter MLD). If we except the area of small MLD located near 41°N, 19.5°W, which is linked to the fingerprint of the cyclonic cold-core eddy C4 on air–sea fluxes [*Bourras et al.*, 2004], the MLD field is quite close to a south-north gradient in expREF (Figure 3). This result is even stronger if we consider the maximum MLD field (not shown). There is indeed a relatively strong gradient located near 42°N in this field, lifelike the one usually found in lower resolution studies [e.g., *Williams et al.*, 1995; *Valdivieso Da Costa et al.*, 2005]. To the contrary, the MLD field as well as the maximum MLD field (not shown) is far from amounting to a simple south–north gradient in expMESO (Figure 3). In this experiment, the MLD field is filament shaped as is the vertical velocity field, but to a lesser extent, and some structures are persistent during a few days, particularly during the restratification period. Note that the MLD is computed using a potential density finite difference criterion. This method has been retained as the most suitable one in the context of the POMME program. In particular, it is more stable than the others, as has already been noted by *Brainerd and Gregg* [1995], and stability is of primary importance for the mixed layer budget calculations presented in this article. The reference depth is set at the third z-level (12.5 m) to limit diurnal cycle effects, and the density threshold is 0.023 kg m^{-3}, close to the values found in the recent extensive study of *Boyer Montégut (de) et al.* [2004].

[20] The mesoscale and submesoscale structures revealed by expMESO lead us to this question: Do they have an effect on the processes occurring in the mixed layer in the POMME area, and if they do, which one? In the following sections, the simulations expREF and expMESO will provide the material to answer this question in a much more comprehensive way than what would have been possible using the data alone. But first, let us consider the domain-averaged mixed layer depth (Figure 4). The domain-averaged MLD maximum occurs around 4 March in expREF. It occurs a bit earlier in expMESO, around 1 March. The domain-averaged MLD is also significantly smaller in expMESO than in expREF from 1 March to 25 March, with a difference reaching 22 m on 10 March. Therefore an earlier and more intense restratification occurs in expMESO from 1 March to 25 March. This difference can be attributed to the role of mesoscale eddies in the restratification [e.g., *Lévy et al.*, 1998; *Nurser and Zhang*, 2000; *Oschlies*, 2002; *Henning and Vallis*, 2005], but also to the effect of the submesoscale filaments induced by mesoscale eddies. Indeed, *Lapeyre et al.* [2006] found that the surface frontogenesis, induced by the stirring of density fronts near the surface, increases the stratification in the upper ocean. Here vertical velocities in the upper ocean, which are at least partly related to the submesoscale ageostrophic circulations that develop to counteract the growth of horizontal density gradients, are the most intense from 1 March to 25 March in the POMME area [*Paci et al.*, 2005]. Note that this effect of the submesoscale filaments might be slightly underestimated in our simulation due to their small size relative to the model resolution.

3. Heat Budget

[21] A heat budget analysis has been performed in both simulations in order to investigate the effect of mesoscale eddies on the physical processes contributing to mixed layer and sea surface temperature variations.

3.1. Formulation

[22] The budget equation is derived from the full model equation for the tracer X, namely, temperature or salinity:

$$\partial_t X = -U \cdot \nabla X - w\partial_z X + \partial_z F_p - \partial_z \overline{X'w'} - \nabla\left(\overline{X' \cdot U'}\right) \quad (1)$$

and the continuity equation:

$$\nabla \cdot U + \partial_z w = 0 \quad (2)$$

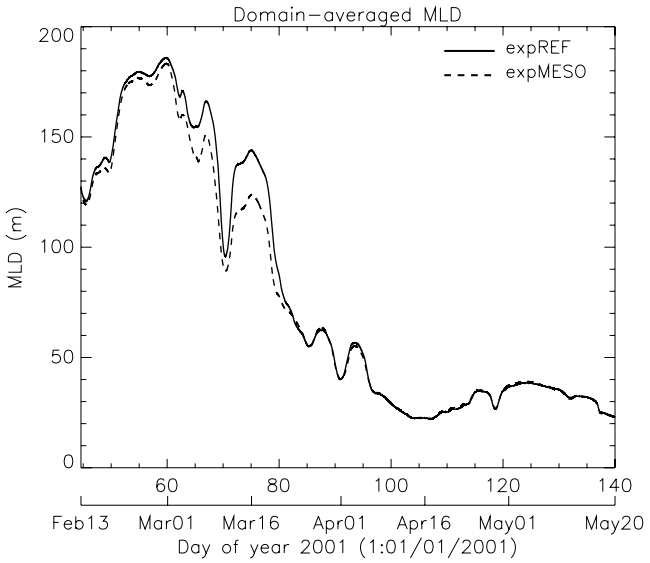

Figure 4. Temporal evolution of the domain-averaged mixed layer depth in expREF (plain line) and in expMESO (dashed-line). Under the effect of mesoscale eddies, the restratification occurs 3 days earlier and is more intense from 1 March to 25 March.

[23] $U = (u,v)$ is the horizontal velocity component, w is the vertical velocity component, $\partial_z F_p$ is the depth derivative of the penetrative flux of X, $\overline{U'X'}$ and $\overline{w'X'}$ are the horizontal and vertical part, respectively, of the turbulent flux of X, and $\nabla \equiv (\frac{\partial}{\partial x}, \frac{\partial}{\partial y})$. The overbar averaging operator is a Reynolds average. It allows the resolution of the motion and timescales of interest without simulating the significantly smaller ones. This operator is applied on each variable of the model. But, for the sake of simplicity, the overbar has been kept only for the turbulent fluxes (i.e. fluxes associated with the average correlation of turbulent fluctuations over the meshgrid and timestep of the model). These turbulent fluxes are represented with diffusive closure schemes.

[24] We define the vertical average of any variable a over the mixed layer as

$$\langle a \rangle = \frac{1}{h}\int_{-h}^{0} a dz \tag{3}$$

where h is the MLD, and then the deviation from this average is $\tilde{a} = a - \langle a \rangle$.

[25] Using the continuity equation and the rigid-lid approximation, the vertical integral of equation (1) becomes:

$$\int_{-h}^{0} \partial_t X dz = -\int_{-h}^{0} \nabla U X dz + w(-h)X(-h) + \left[F_p(0) - F_p(-h)\right] - \overline{w'X'}(0) + \overline{w'X'}(-h) - \int_{-h}^{0} \nabla\left(\overline{X' \cdot U'}\right) dz \tag{4}$$

[26] The vertical integration from $z = -h$ to the surface of the continuity equation leads to:

$$\nabla \cdot \int_{-h}^{0} U dz = \nabla(h\langle U \rangle) = w(-h) + U(-h) \cdot \nabla h \tag{5}$$

[27] Specifying the surface turbulent fluxes as $-\overline{X'w'}(0) = F_{\mathrm{np}}$ (nonpenetrative flux of X), the vertical integral of equation (1) becomes:

$$h\partial_t\langle X \rangle = \underbrace{-h\langle U \rangle \cdot \nabla \langle X \rangle - \nabla \cdot \int_{-h}^{0} \tilde{U}\tilde{X} dz}_{\text{horizontal advection}} \underbrace{-[\langle X \rangle - X(-h)]w_e(-h)}_{\text{entrainment}} \underbrace{+\left[F_p(0) - F_p(-h)\right] + F_{\mathrm{np}}}_{\text{surface flux}} \underbrace{+\overline{w'X'}(-h)}_{\text{vertical diffusion}} \underbrace{-\int_{-h}^{0} \nabla\left(\overline{X' \cdot U'}\right) dz}_{\text{horizontal diffusion}} \tag{6}$$

where $w_e(-h) = w(-h) + U(-h)\cdot\nabla h + \partial_t h$ is defined as the vertical flow of material across the surface $z = -h$. Note that deepening (shallowing) has a positive (negative) contribution to $w_e(-h)$. A quite similar budget equation was derived for temperature by *Stevenson and Niiler* [1983] and *Caniaux and Planton* [1998].

[28] The terms on the right hand side represent, respectively, the horizontal advection of X by the depth-averaged current and by the deviations from this mean current (the sum of these two terms will be called the horizontal advection later on), the flux of X carried by the mean flow across the $z = -h$ surface (defined as the entrainment), the penetrative flux of X, the turbulent fluxes across the upper and $z = -h$ surfaces, and the horizontal diffusion of X. The turbulent fluxes across the $z = -h$ surface (the mixed layer bottom) will be referred to as the vertical diffusion (at the mixed layer bottom).

[29] In the case of the heat budget ($X \equiv T$):

[30] • $[F_p(0) - F_p(-h)] \equiv \frac{F_{\mathrm{sol}}}{\rho_0 c_p}[I(0) - I(-h)]$, where F_{sol} is the short-wave radiative flux at the sea surface, I the fraction of F_{sol} that penetrates to depth z, ρ_0 is the ocean density of reference, and c_p is the ocean specific heat;

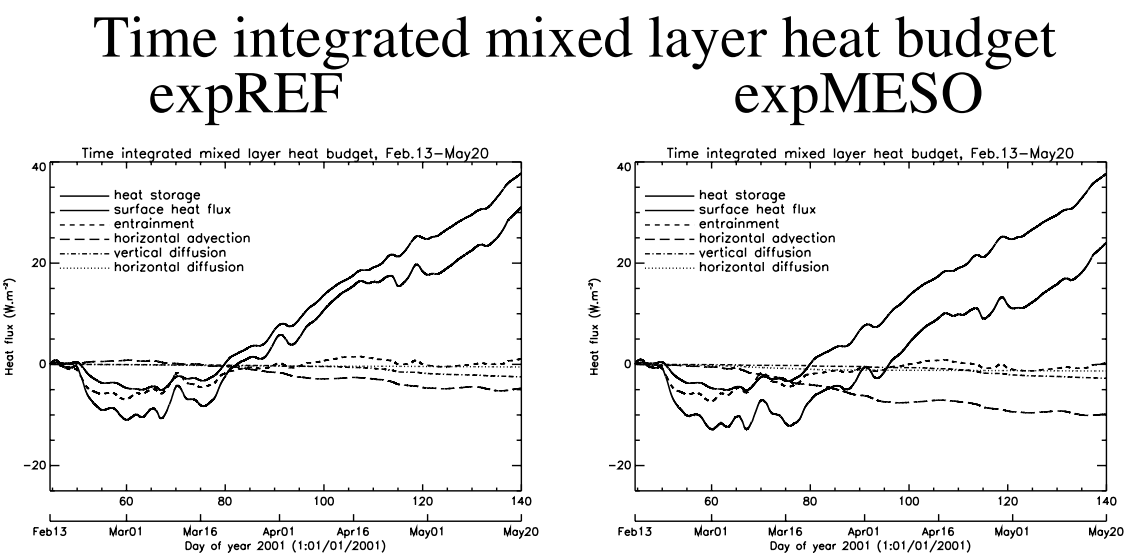

Figure 5. Time-integrated mixed layer heat budget divided by the duration of the experiment for expREF and expMESO. Final values (on 20 May) correspond to the mixed layer heat budget averaged over the duration of the experiment. Surface heat flux and horizontal advection are the main components of heat storage. The horizontal advection of cold water is enhanced by mesoscale eddies.

[31] • $F_{\mathrm{np}} \equiv \frac{F_{nsol}}{\rho_0 c_p}$, where $F_{n\mathrm{sol}}$ is the sum of the sensible (H_{S}), latent (L_{E}), and net infrared heat fluxes (F_{ir});

[32] • the left hand side of equation (6) is the contribution of the depth-averaged temperature to changes in the heat content and will be referred to as the heat storage term. This term gives information about mixed layer and therefore sea surface temperature variation rate.

[33] The sum of the solar penetrative flux and turbulent fluxes across the upper surface will be referred to as the net surface heat flux. Each term of the heat budget has been computed at each time step of the model integration and multiplied by $\rho_0 c_p$ in order to be converted to watts per square meter. All these terms were then time or space averaged. However, because of the damping term near the recirculation area and its nonphysical significance, space averaging was performed on a 105 × 125 inner points subdomain. This area extends from 15.73°W to 20.93°W and from 38.4°N to 44.6°N, representing approximately a 600 × 700 km^2 domain.

3.2. Domain-Averaged Mixed Layer Heat Budget

[34] Time-integrated mixed layer heat budgets are presented in Figure 5 for expREF and expMESO. The values are divided by the duration of the experiment, therefore final values (on 20 May) correspond to the averaged mixed layer heat budget from 13 February to 20 May. Surface heat flux and horizontal advection are the main components of the heat budget over the duration of the experiments. Moreover, the temporal high frequency of the heat storage is driven by the surface heat flux. Whereas surface heat flux warms the mixed layer at a mean rate of about 38 W m^{-2}, all the other terms act to cool it (excepted entrainment that is very small although positive) in both experiments. As a whole, heat storage increases at a mean rate of 31 W m^{-2} in expREF and 24 W m^{-2} in expMESO. This difference is explained by a horizontal advection of cold water, which is increased by more than 100% by mesoscale eddies, mostly during the restratification period. If the cooling effect of horizontal advection represents only 12% of the surface heat flux in expREF, it represents more than 25% of the surface heat flux in expMESO. Thus, if the mixed layer is thinner in expMESO than in expREF during the restratification under the effect of mesoscale eddies, it is not overheated relatively to expREF because the horizontal advection of cold water in the mixed layer is also enhanced by mesoscale eddies. This horizontal advection counteracts the shallowing of the mixed layer by mesoscale eddies. In fact, the increase of SST is slightly lower in expMESO than in expREF (by 0.04°C) over the duration of the experiments, and final SST is closer to the data in expMESO than in expREF.

[35] In the two experiments, the cooling effect of total horizontal advection is the result of a meridional advection of cold water and a smaller zonal advection of warm water. Both are enhanced by mesoscale eddies, but the effect is stronger for the meridional advection (×2.4) than for the zonal advection (×1.8).

3.3. Spatial Variability of the Mixed Layer Heat Budget

[36] The two-dimensional heat storage, horizontal advection, and net surface heat flux averaged over the 13 February to 20 May period are presented in Figure 6 for expREF and expMESO. The other two-dimensional fields of heat budget terms are less significant relative to the spatial variability of the heat storage. The net surface heat flux field contains fingerprints of oceanic mesoscale eddies, but the horizontal advection is counteracting these mesoscale structures and the resulting heat storage field is very homogeneous in expREF. To the contrary, the heat storage field contains very contrasted mesoscale and submesoscale structures in expMESO. In this experiment, the heat storage is shaped by mesoscale eddies through the horizontal advection. Structures of intense cold and warm horizontal advection are located at fronts between eddies. This has been also

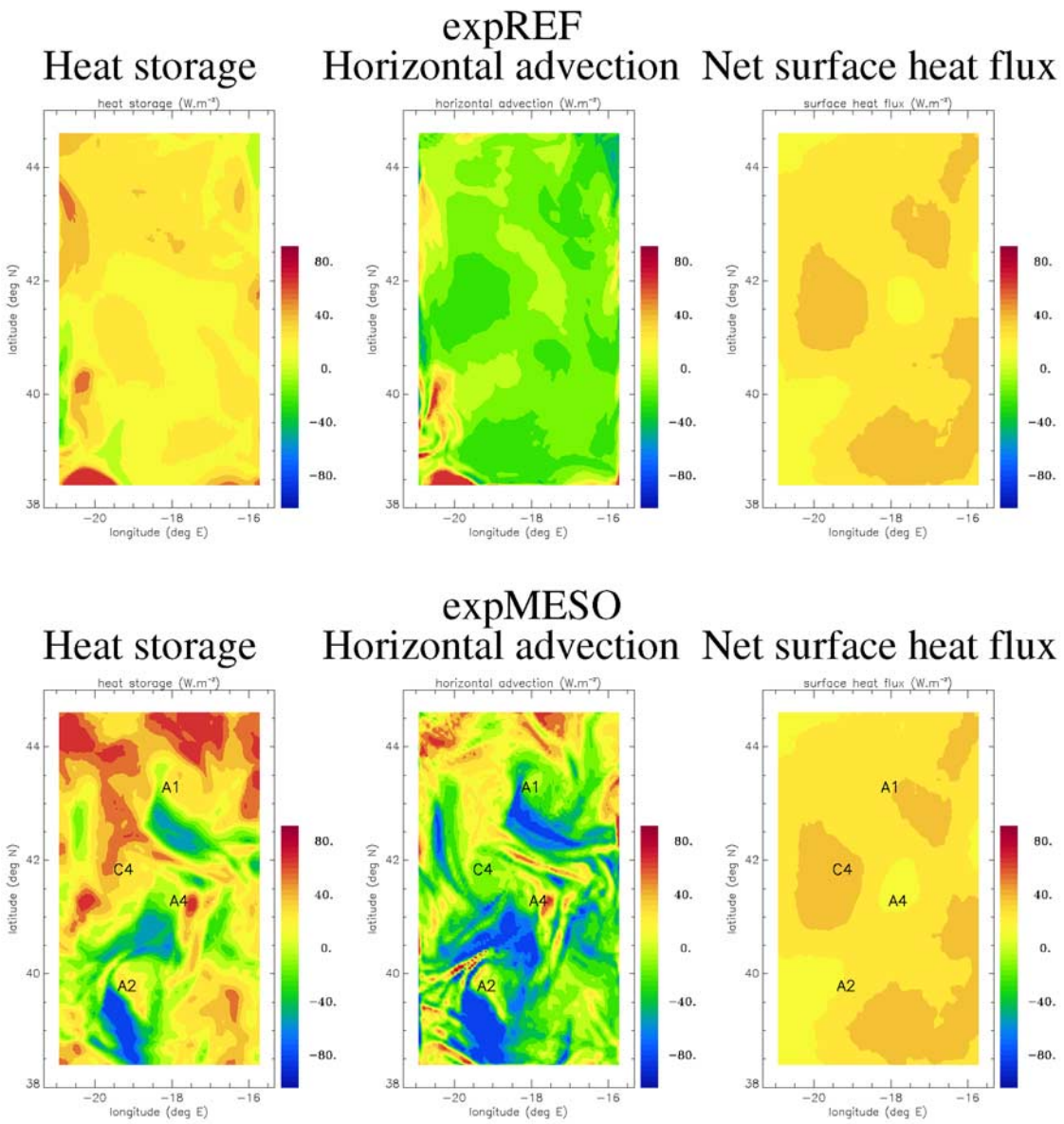

Figure 6. Synoptic charts of 96 daytime-averaged heat storage, horizontal advection, and net surface heat flux (13 February to 20 May) for expREF and expMESO. Units are $W\,m^{-2}$. The heat storage is shaped by mesoscale eddies through the horizontal advection. The structures of cold horizontal advection are stronger and larger than the warms ones, which is responsible for the cooling effect of mesoscale eddies.

reported in *Caniaux and Planton* [1998] and *Giordani et al.* [2005b]. It is interesting to point out that these structures developed mainly during the restratification period. The structures of cold horizontal advection are stronger and larger than the warm ones, which is responsible for the cooling effect of mesoscale eddies. They are located mainly on the southern side of A1 (anticyclonic cold-core eddy) and A2 (anticyclonic warm-core eddy) and between A2 and C4 (cyclonic cold-core eddy).

4. Salt Budget

[37] A salt budget analysis has been also performed in the two simulations in order to investigate the effect of mesoscale eddies on the physical processes contributing to mixed layer and sea surface salinity variations. The formulation and calculation are similar to the ones presented for the heat budget in section 3.1.

4.1. Formulation

[38] In the case of the salt budget $X \equiv S$ in equation (6) and:

[39] • $[F_p(0) - F_p(-h)] \equiv 0$, as there is no penetrative flux of salt;

[40] • $F_{\mathrm{np}} \equiv (E - P)\mathrm{SSS}$, where E is the evaporation rate, P is the precipitation rate, and SSS is the sea surface salinity, will be referred to as the net evaporation flux;

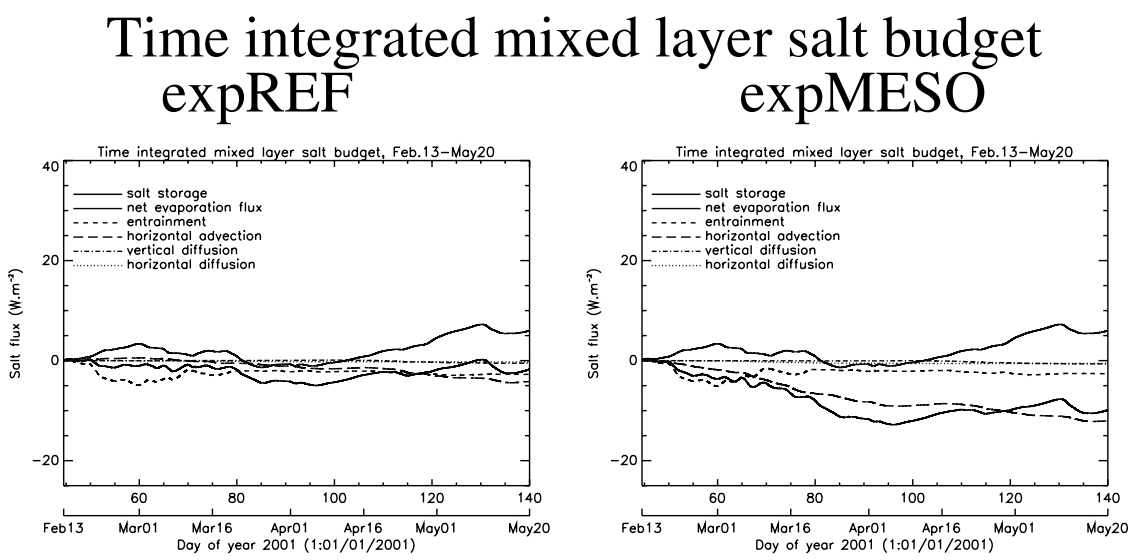

Figure 7. Time-integrated mixed layer salt budget divided by the duration of the experiment for expREF and expMESO. Final values (on 20 May) correspond to the mixed layer salt budget averaged over the duration of the experiment. Horizontal advection and surface salt flux are the main components of salt storage. The horizontal advection of freshwater is enhanced by mesoscale eddies. Note that -10 W m^{-2} is equivalent to an addition of approximately 1 mm day^{-1} of freshwater.

[41] • the left hand side of equation (6) is the contribution of the depth-averaged salinity to changes in the salt content and will be referred to as the salt storage term. This term gives information about mixed layer and therefore sea surface salinity variation rate.

[42] Each term of the salt budget has been multiplied by $\rho_0 c_p \frac{\beta}{\alpha}$ in order to be converted to their equivalent in watts per square meter. α is the thermal expansion coefficient and β is the haline contraction coefficient. The value retained is a constant $\frac{\beta}{\alpha} = 5$ K. This procedure allows to compare heat and salt budgets in relation to the relative contribution of T and S in the equation of state, i.e. to their respective contribution to the variation of the seawater density.

4.2. Domain-Averaged Mixed Layer Salt Budget

[43] Time-integrated mixed layer salt budget is presented in Figure 7 for expREF and expMESO. As in section 3.2, the values are divided by the duration of the experiment, therefore final values (on 20 May) correspond to the averaged mixed layer salt budget from 13 February to 20 May. Horizontal advection and surface salt flux are the main components of the salt budget over the duration of the experiments. Moreover, the temporal high frequency of the salt storage is driven by the net evaporation flux. Whereas the net evaporation flux tends to increase the salt storage at a mean rate of about 6 W m^{-2} (this means that the evaporation rate exceeds the precipitation rate by about 0.6 mm day^{-1}), all the other terms act to decrease it. As a whole, salt storage decreases at a mean rate of 1.6 W m^{-2} in expREF and 9.7 W m^{-2} in expMESO. This difference is explained by a horizontal advection of freshwater, which is increased by nearly 300% by mesoscale eddies, mostly during the restratification period. If the freshening effect of horizontal advection represents 68% of the surface salt flux in expREF, it is about two times larger than the surface heat flux in expMESO. Therefore if the mixed layer is thinner in expMESO than in expREF during the restratification under the effect of mesoscale eddies, it is not oversalted relatively to expREF because the horizontal advection of freshwater in the mixed layer is also enhanced by mesoscale eddies. However, the increase of SSS is slightly higher in expMESO than in expREF (by 0.013) over the duration of the experiments.

[44] In the two experiments, the freshening effect of total horizontal advection is the result of a meridional advection of freshwater and a small zonal advection of salty water. The effect of mesoscale eddies on the total horizontal advection is mainly due to an enhancement of the meridional advection of freshwater ($\times 2.22$).

[45] As for the mixed layer heat budget, the main components of salt budget are surface flux and horizontal advection. Nevertheless, horizontal advection is relatively more important for the salt budget than for the heat budget, it is even the main term of the salt budget under the influence of mesoscale eddies.

4.3. Spatial Variability of the Mixed Layer Salt Budget

[46] The results regarding the two-dimensional fields of salt budget terms averaged over the 13 February to 20 May period (not shown) are quite similar to the ones found for the heat budget. However, in this case the mesoscale structures of the net surface salt flux are too weak to have an impact on the spatial variability of the horizontal advection and salt storage terms, even in expREF. In this experiment, the horizontal advection field is very homogeneous as is the salt storage field. To the contrary, the salt storage field contains very contrasted mesoscale and submesoscale structures in expMESO. In this experiment, the spatial variability of the horizontal advection and salt storage terms is very similar to the spatial variability of the corresponding fields presented in Figure 6 for the heat budget. In particular, the structures of horizontal advection

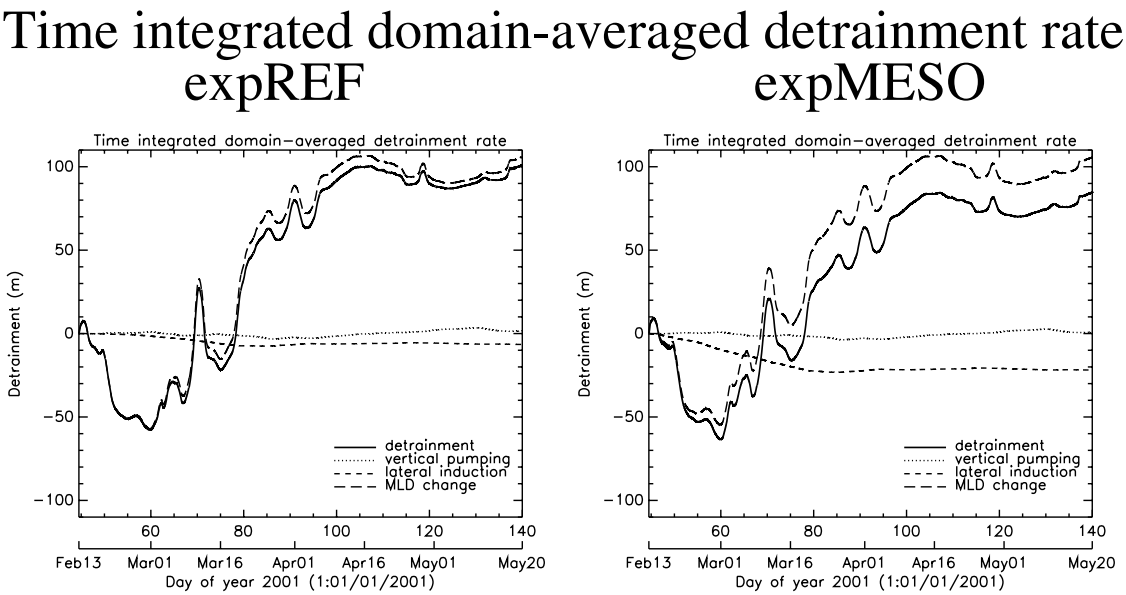

Figure 8. Time-integrated domain-averaged detrainment rate for expREF and expMESO. A positive value means that at the given time (horizontal axis) the amount of water in meters reads on the vertical axis has left the mixed layer over the domain in average since the beginning of the experiment. The respective contribution of vertical pumping, lateral induction, and MLD change in the detrainment is also shown. Mesoscale eddies induce a significant entrainment by lateral induction. The resulting detrainment appears to be reduced by more than 15%.

of freshwater are stronger and larger, which is responsible for the freshening effect of mesoscale eddies. As for the heat budget, these structures developed mainly during the restratification period.

5. Mixed Layer/Pycnocline Water Exchange

5.1. Formulation

[47] The flux of water across the base of the mixed layer toward the pycnocline is termed detrainment, whereas the flux of water across the base of the mixed layer toward the mixed layer is termed entrainment [*Qiu and Huang*, 1995]. The instant detrainment rate [e.g., *Cushman-Roisin*, 1987] is defined by:

$$D = -(w(-h) + u(-h).\nabla h + \partial_t h) \tag{7}$$

where h is the mixed layer depth. When $D > 0$ water is effectively detrained from the mixed layer to the pycnocline, whereas when $D < 0$ water is effectively entrained from the pycnocline to the mixed layer. Note that D is equal to the opposite of $w_e(-h)$, as it is defined in section 3.1.

[48] Following *Tsujino and Yasuda* [2004], the first term on the right-hand side of equation (7) will be called the vertical pumping, the second term will be called the lateral induction, and the last term will be called the MLD change. Each term has been computed at each time step of the model, and then these terms were then time or space averaged. As in sections 3 and 4, space averaging was performed in the physical domain (the damping area is excluded).

5.2. Domain-Averaged Detrainment

[49] Time-integrated domain-averaged detrainment rates are presented in Figure 8 for expREF and expMESO. If the detrainment is largely dominated by the MLD change in expREF, the lateral induction has also a significant contribution in expMESO due to an increase by mesoscale eddies of the amount of water entrained into the mixed layer by this process. This amount of water is more than three times larger in expMESO than in expREF. Lateral induction and the effect of mesoscale eddies on it occur mainly from the beginning of the simulation to the end of the first half of the restratification period (about 20 March). Note that lateral induction is negative in expMESO, which is opposite to what is expected from a large-scale southward current [e.g., *Paillet and Arhan*, 1996a, 1996b]. Actually the meridional lateral induction is positive, which is consistent with a southward current, but the total lateral induction is dominated by a negative zonal lateral induction. Vertical pumping is small in the two experiments, but it is smaller in expMESO (1 m) than in expREF (1.8 m). As the MLD change is the same in the two experiments, the resulting detrainment appears to be reduced by more than 15% by mesoscale eddies. This is consistent with the results of *Valdivieso Da Costa et al.* [2005], which found that eddies tend to counteract the detrainment by the mean flow, reducing the total annual subduction rate in the density class of interest (26.8–27.2) in the northeast Atlantic. But it is opposed to what they found in the particular POMME area (see Figure 9f in their article). This may be attributed to interannual variability, as their work is based on a 20-year average of the model fields. It may also be attributed to the lower resolution of their study. Over the duration of the experiment (96 days), the domain-averaged amount of water leaving the mixed layer is about 85 m in expMESO, in very good agreement with the results obtained from a different numerical model by *Giordani et al.* [2005b].

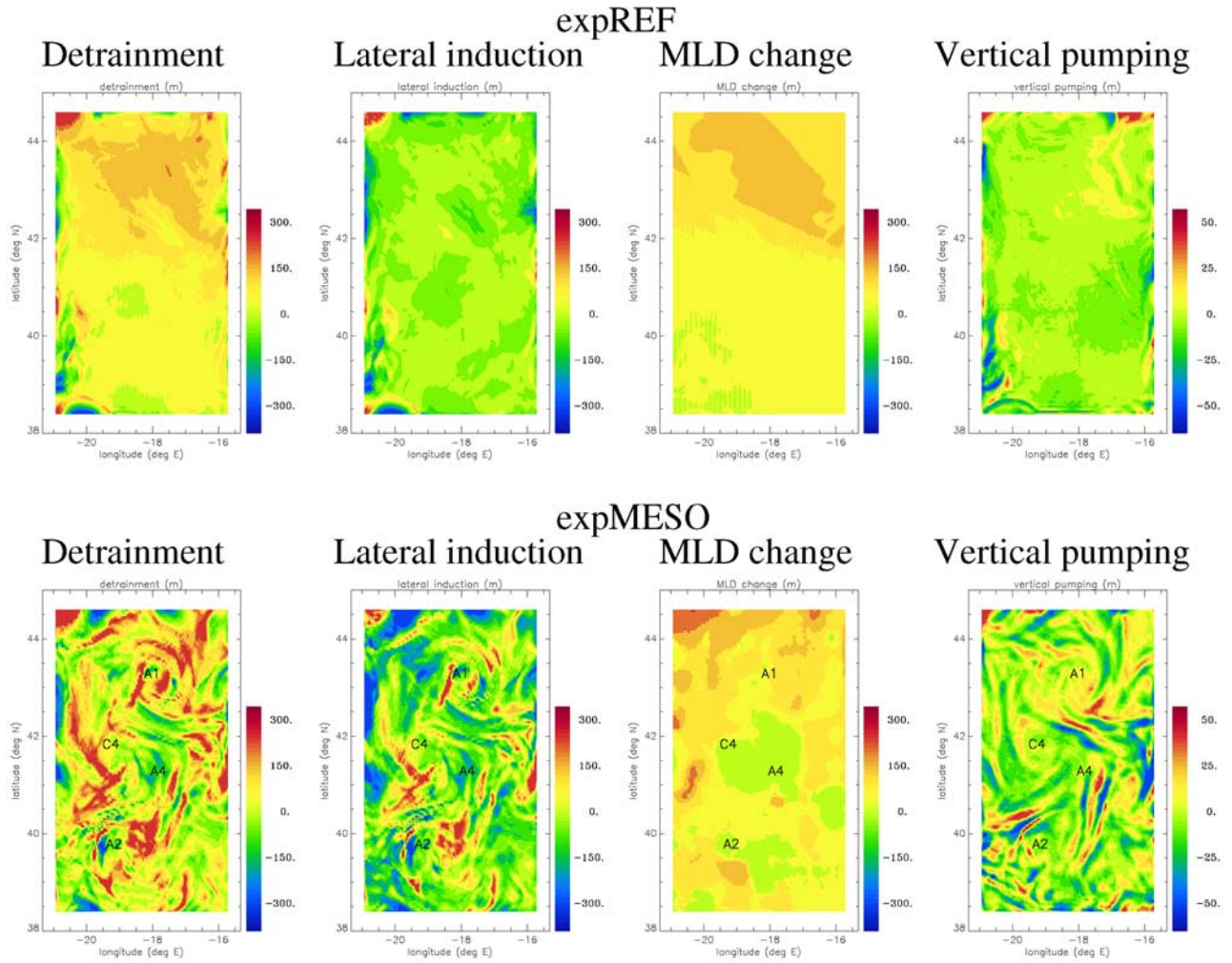

Figure 9. Synoptic charts of 96 daytime-cumulated vertical pumping, lateral induction, MLD change, and resulting detrainment (13 February to 20 May) for expREF and expMESO. Units are meters. Note that the scale used for vertical pumping is six times smaller than the one used for the other fields. If the domain-averaged effect of mesoscale eddies on the lateral induction is to entrain more water into the mixed layer, eddies contribute to detrain water in the peculiar positive filaments seen on this field in expMESO.

5.3. Spatial Variability of the Detrainment

[50] Two-dimensional fields of detrainment terms averaged over the 13 February to 20 May period are presented in Figure 9 for expREF and expMESO. Detrainment in expREF is a positive field, with higher values north of 42°N, as is the MLD change field. This field is actually very similar to the annual subduction rate field found in the lower resolution study of *Valdivieso Da Costa et al.* [2005] in the POMME area (see Figure 9d in their article). Lateral induction and vertical pumping have not a significant contribution to the spatial variability of the detrainment in expREF. To the contrary, lateral induction in expMESO is a very contrasted field, dominated by some submesoscale filaments of intense positive lateral induction and more numerous areas of moderate to intense negative lateral induction. The filaments are related to the structures seen on the MLD fields during the restratification period (see Figure 3). If the domain-averaged effect of mesoscale eddies on lateral induction is to entrain more water into the mixed layer, eddies contribute to detrain water in these peculiar filaments. The resulting detrainment field has the shape of the lateral induction field but shifted toward positive values by the MLD change term, which is quite homogeneous relatively to the other fields. Even if it does not contribute much to the spatial variability of the detrainment, the vertical pumping also exhibits filament-shaped structures in expMESO but less intense than in the lateral induction field. These submesoscale structures are associated as dipoles of positive and negative vertical pumping, in the fronts between eddies. Filaments of negative vertical pumping are more numerous than filaments of positive vertical pumping, which is responsible for the effect of mesoscale eddies on the domain-averaged field.

5.4. Detrainment in Individual Density Classes

[51] Besides the previous results regarding the detrainment term taken as a whole, it is important to know how this term splits on individual density classes. Detrainment and entrainment through the mixed layer base at $0.1\sigma_\theta$ intervals over the POMME domain (damping area excluded) from 13 February to 01 March are presented in Figure 10 for expREF and expMESO. They are calculated as a function of density classes following instantaneous isopycnal positions in the mixed layer in equation (7). The net exchanged water through the mixed layer base (net detrainment) is also represented.

[52] The first effect of mesoscale eddies is to enhance the real exchange of water between the mixed layer and the pycnocline (white bars in Figure 10): the amount of detrained water increases by about 40% and the amount of entrained water increases by nearly 60% in expMESO relatively to expREF. According to sections 5.2 and 5.3, this is mainly due to the lateral induction, and the resulting net detrainment is reduced by about 15%. But Figure 10 shows that the decrease of the net detrainment by mesoscale eddies is far from being homogeneously distributed among the individual density classes. To the contrary, the effect of mesoscale eddies on the net detrainment impacts mainly two potential density classes: 26.85–26.95 and 26.95–27.05. In fact, if mesoscale eddies contribute to entrain about 30 m of water into the mixed layer in the 26.85–26.95 density class, they also detrain about 15 m of water from the mixed layer to the pycnocline in the 26.95–27.05 density class. This is a result of primary importance because these density classes, in particular the second one, are likely to be the ones involved in the formation of subpolar mode water during the POMME experiment according to *Reverdin et al.* [2005] and to the results of ongoing research conducted on the high-resolution in situ data collected during P2L2.

[53] In order to better understand these effects of mesoscale eddies, it is interesting to consider the synoptic charts of the difference between expMESO and expREF in the detrainment of these two density classes. They are presented in Figure 11. In the 26.85–26.95 density class, the area of detrainment by MLD change north of 42°N (Figure 9) is weaker in expMESO than in expREF, hence the entrainment effect of mesoscale eddies. This is related to the earlier and more intense restratification induced by mesoscale eddies. Indeed, this effect of mesoscale eddies affects the mixed layer density during the first half of the restratification, which has an influence on the characteristics of the detrained water. This is consistent with the numerical results of *Valdivieso Da Costa et al.* [2005]. They suggest indeed that the change in the mixed layer density during the period of effective detrainment has an important impact on the subduction. However, there are some filaments of detrainment by lateral induction on the western side of C4, between C4 and A4, and south of A4. These filaments are related to the advection of cold (and fresh) water in the mixed layer seen in Figure 6, under the horizontal velocity field induced by these mesoscale eddies. Part of this water is likely to come from outside of the POMME area, in particular on the western lateral boundary near 40°N, where a weak surface intensified eastward flow has been revealed from the subsurface floats [*Le Cann et al.*, 2005].

[54] The anticyclonic eddy A1 is the key element for the detrainment of the 26.95–27.05 density class. On the one hand, it is responsible for the horizontal advection of denser (cold and fresh, but the temperature effect prevails) in the mixed layer from the northern lateral boundary near 18°W and 16.5°W. Part of this water is winding round A1, as seen in Figure 6. On the other hand, it is responsible for the detrainment by lateral induction of this advected water. Note also that some of the water detrained in the vicinity of A1 had been probably advected within the eddy during its propagation in the ocean. Moreover, there is some detrained water advected from the north near 16.5°W by A1 in the density range 27.05–27.10 (not shown). The water advected from the north and detrained in the POMME area by the anticyclonic eddy A1 has a smaller probability to be entrained again into the mixed layer during the following winter. Therefore this water has more chance to be effectively subducted in the POMME area than if it would have been detrained farther north. These results are confirmed by in situ data. Filament-shaped structures of high oxygen, similar to the simulated filaments of detrainment, were found in the high-resolution survey carried out during P2L2 on the region south of the anticyclonic eddy A1 [e.g., *Reverdin et al.*, 2005, p. 14]. An area of high oxygen was also found in the region east of A1 [*Reverdin et al.*, 2005, pp. 7–8]. Moreover, evidence of a deep oxygen maximum was found in the core of A1 [*Le Cann et al.*, 2005, p. 19], suggesting that this eddy has indeed a very particular effect on the detrainment. J. C. Gascard et al. (unpublished data, 2005) found also that this eddy may contain some newly ventilated water. These results are consistent with the data analyzed by *Paillet* [1999], which indicate that significantly more anticyclones than cyclones contain mode water in the north of the area.

6. Conclusion

[55] According to the traditional standpoint [*Paillet and Arhan*, 1996a], subduction in the POMME area is explained by a lateral induction of water by a mean southward velocity of about 1 cm s^{-1} (as retained by *van Aken* [2001]) across a steep MLD gradient (as seen in *Williams et al.* [1995] and *Valdivieso Da Costa et al.* [2005]). If this had been observed, it would have been quite easy to evaluate the subduction in the area from the value of the meridional current and the MLD field. But the mesoscale eddies were much more numerous in this relatively quiescent region of the ocean than previously reported by *Paillet* [1999]. In fact, the circulation is dominated by mesoscale eddies, with little indication of such a mean southward current [*Reverdin et al.*, 2005], and the MLD distribution does not present a steep gradient [*Paci et al.*, 2005]. In order to assess the effect of these mesoscale eddies, a high-resolution simulation has been performed during a key period of the POMME experiment (POMME 1 and POMME 2, late Winter and Spring of 2001). This period contains the period of effective detrainment as defined by *Qiu and Huang* [1995], indeed the effective detrainment takes place after late winter when the mixed layer reaches its annual maximum depth and starts to retreat. The amount of detrainment during this period controls the annual subduction rate, as well as the characteristics of the subducted water. The simulation

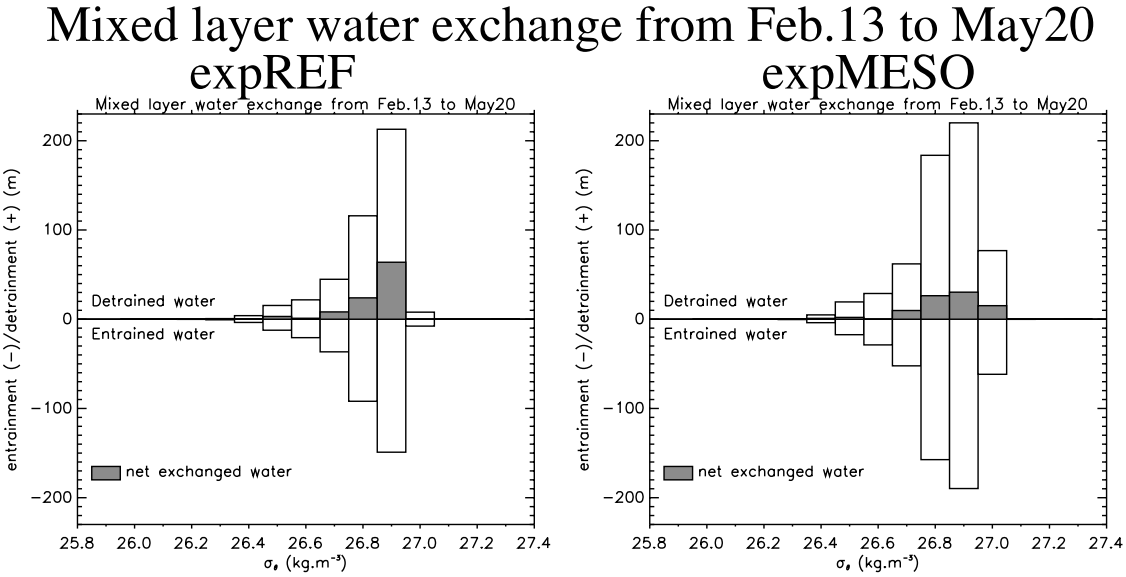

Figure 10. Detrainment (positive white bars) and entrainment (negative white bars) through the mixed layer base in meters at 0.1 σ_θ intervals over the POMME domain (damping area excluded) from 13 February to 01 March for expREF and expMESO. The net exchanged water through the mixed layer base is represented by grey tone bars. If mesoscale eddies contribute to entrain about 30 m of water into the mixed layer in the 26.85–26.95 density class, they also detrain about 15 m of water from the mixed layer to the pycnocline in the 26.95–27.05 density class.

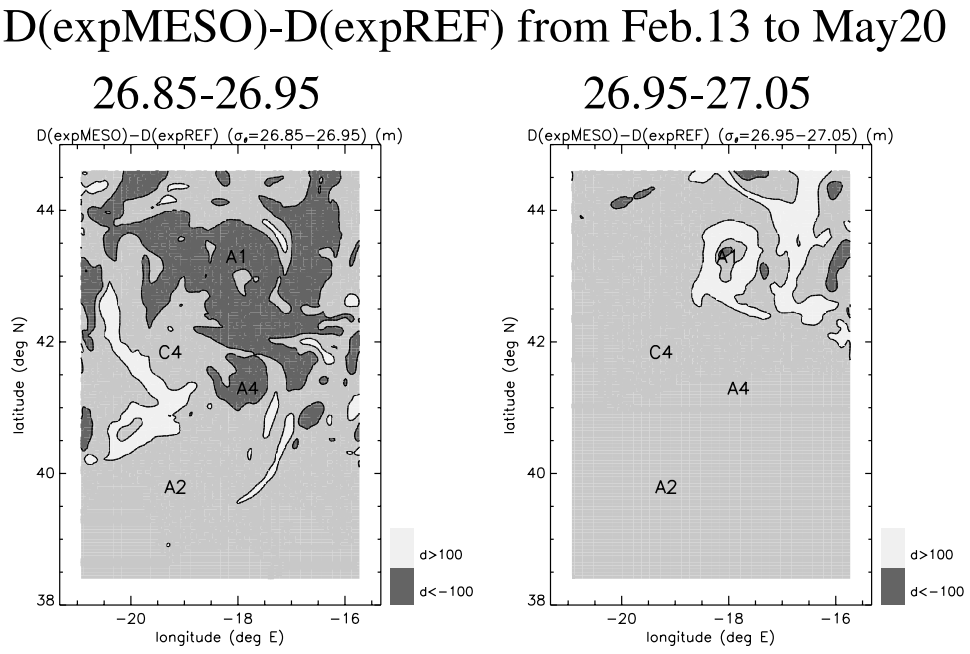

Figure 11. Synoptic chart of 96 (13 February to 20 May) daytime-cumulated detrainment in expMESO minus the same field in expREF. The fields are plotted for the two major σ_θ intervals that may be involved in the formation of subpolar mode water during the POMME experiment. They highlight the role of the mesoscale eddies in the detrainment of these density classes. The white areas correspond to a difference larger than 100 m, whereas the dark grey areas correspond to a difference smaller than −100 m.

results have been carefully compared with the extensive data set collected during P1 and P2, including temperature, salinity, and horizontal currents measurements. This validation work shows the good quality of the simulation and its ability to properly represent the large-scale gradients in the area as well as the mesoscale features. A second simulation, without mesoscale eddies, is used as a reference to be compared with this simulation through mixed layer heat, salt, and water budgets.

[56] Besides their imprint on the horizontal currents, mesoscale eddies induce the development of filament-shaped vertical velocity and mixed layer depth structures. These mesoscale and submesoscale features have a strong impact on the spatial variability of the mixed layer budgets. The two-dimensional structure of the surface heat and freshwater fluxes is not found in the two-dimensional structure of the storage terms because the temperature and salinity are redistributed by mesoscale eddies through the horizontal advection. Similarly, the two-dimensional structure of detrainment is not retrieved from the two-dimensional structure of the MLD change but is controlled by the lateral induction induced by mesoscale eddies. These phenomena occur during the period of evolving MLD, particularly during the restratification period, and underline the importance of the complex interaction between mesoscale eddies and MLD evolution. The fact that mesoscale and submesoscale structures have a strong and clear signature on the spatial variability of the budgets is not only due to the slow evolution of mesoscale eddies during the duration of the experiment. It also suggests that the structures present during periods of rapid MLD evolution have the strongest influence on the spatial variability of the processes.

[57] The effect of these structures on the domain-averaged mixed layer budgets is far from being negligible. At the domain scale, air–sea fluxes and horizontal advection are the leading terms in the heat budget and salt budget, respectively. Similarly, the domain-averaged detrainment is controlled by MLD change and lateral induction. Mesoscale eddies account for a significant part of these budgets through the horizontal advective terms. Indeed, they represent 52% and 66% of the horizontal advection of temperature and salinity, respectively, and 70% of the lateral induction. As observed for the spatial variability of the budgets, the effect of mesoscale eddies occurs mainly during the period of MLD evolution, in particular during the restratification. Actually, according to the comparison with the study of *Giordani et al.* [2005b], it seems that mesoscale activity during the restratification has a major influence on the annual budgets.

[58] These results have important consequences for the exchange of water between the mixed layer and the pycnocline. Detrainment appears to be reduced by more than 15% by mesoscale eddies. If the water detrained over the duration of the experiment was effectively detrained over a year, it would correspond to an annually averaged net detrainment rate of about 0.8 Sv (1 Sv is 10^6 m^3 s^{-1}). It would be consistent with the results of *Valdivieso Da Costa et al.* [2005], *Gaillard et al.* [2005], and *Giordani et al.* [2005b], where values ranging between 0 and 1.4 Sv were obtained in the POMME area. But more important are the results relative to the distribution over the density classes of the detrained water. Indeed, mesoscale eddies increase the density of the detrained water by two mechanisms. The first involves a particular anticyclonic eddy, A1, located in the north of the domain. Under the influence of this eddy, there is a horizontal advection of northern dense water that is detrained in the domain. The second involves the earlier and more intense restratification induced by mesoscale eddies, resulting in the detrainment of denser water during the period of effective detrainment. This effect of eddies on the density of the detrained water is of primary importance because it leads to the detrainment of water likely to be involved in the formation of subpolar mode water during the POMME experiment. Under the influence of mesoscale eddies, this water is detrained in the POMME area and not farther north; thus, it has a smaller probability to be entrained again into the mixed layer during the following winter, and therefore it has more chance to be effectively subducted in the area.

[59] These results suggest that a realistic numerical study of the intrannual to interannual variability of the upper ocean should use a model able to represent mesoscale eddies and their propagation in the ocean, with some parameterization of the submesoscale dynamics if this is not explicitly resolved.

[60] **Acknowledgments.** The authors are grateful to the Hydrographic Service of the French Navy (SHOM) for the model high-resolution bathymetry, to the OPA system team for their development and maintenance of the LODYC ocean model, and to Youcef Amar for technical support. The altimeter products were produced by the CLS Space Oceanography Division as part of the Environment and Climate EU ENACT project (EVK2-CT2001-00117) and with support from CNES. This study is a contribution to the POMME program managed by Laurent Mémery and Gilles Reverdin. Financial support was provided by the French research programs PATOM and PROOF and the French agencies CNRS, IFREMER, Météo-France, and SHOM. The data used result from a joint effort by all the POMME participants led by the onboard chief scientist Micheline Bianchi, Yves Desaubies, Jean-Claude Gascard, Fréderic Herpers, Patrick Mayzaud, Jérôme Paillet, and Louis Prieur.

References

Bourras, D., G. Reverdin, H. Giordani, and G. Caniaux (2004), Response of the atmospheric boundary layer to a mesoscale oceanic eddy in the northeast Atlantic, *J. Geophys. Res.*, *109*, D18114, doi:10.1029/2004JD004799.

Boyer Montégut de, C., G. Madec, A. S. Fischer, A. Lazar, and D. Iudicone (2004), A global mixed layer depth climatology based on individual profiles, *J. Geophys. Res.*, *109*, C12003, doi:10.1029/2004JC002378.

Brainerd, K. E., and M. C. Gregg (1995), Surface mixed and mixing layer depths, *Deep Sea Res. Part I*, *42*(9), 1521–1543.

Caniaux, G., and S. Planton (1998), A 3D ocean mesoscale simulation using data from the SEMAPHORE experiment: Mixed layer heat budget, *J. Geophys. Res.*, *103*, 25,081–25,099.

Caniaux, G., H. Roquet, and S. Planton (1993), A 3D mesoscale simulation of the ocean using data from the ATHENA88 field experiment, *J. Mar. Sys.*, *4*, 197–216.

Caniaux, G., A. Brut, D. Bourras, H. Giordani, A. Paci, L. Prieur, and G. Reverdin (2005a), A 1 year sea surface heat, freshwater and momentum budget in the northeast Atlantic basin during the POMME experiment. part 1: Flux estimates, *J. Geophys. Res.*, *110*, C07S02, doi:10.1029/2004JC002596.

Caniaux, G., S. Belamari, H. Giordani, A. Paci, L. Prieur, and G. Reverdin (2005b), A one year sea surface heat, freshwater and momentum budget in the northeast Atlantic basin during the POMME experiment. part 2: Flux correction, *J. Geophys. Res.*, *110*, C07S03, doi:10.1029/2004JC002695.

Cushman-Roisin, B. (1987), Subduction, in *Aha Huliko: A Hawaiian Winter Workshop. Dynamics of the oceanic surface mixed layer*, edited by P. Müller and D. Henderson, pp. 181–196, Hawaii Institute of Geophysics Special Publications, University of Hawaii at Manoa, Honolulu.

Gaillard, F., H. Mercier, and C. Kermabon (2005), A synthesis of the POMME physical data set: One year monitoring of the upper mixed layer, *J. Geophys. Res.*, *110*, C07S07, doi:10.1029/2004JC002764.

Gavart, M., P. De Mey, and G. Caniaux (1999), Assimilation of satellite altimeter data in a primitive-equation model of the Azores–Madeira region, *Dyn. Atmos. Oceans*, *29*, 217–254.

Gebbie, G. (2007), Does eddy subduction matter in the northeast Atlantic Ocean?, *J. Geophys. Res.*, in press.

Giordani, H., G. Caniaux, and L. Prieur (2005a), A simplified 3D oceanic model assimilating geostrophic currents: Application to the POMME experiment, *J. Phys. Oceanogr.*, *35*(5), 628–644.

Giordani, H., G. Caniaux, L. Prieur, A. Paci, and S. Giraud (2005b), A one year mesoscale simulation in the northeast Atlantic: Mixed layer heat and detrainment–entrainment budgets during the POMME experiment, *J. Geophys. Res.*, *110*, C07S08, doi:10.1029/2004JC002764.

Giordani, H., G. Caniaux, and L. Prieur (2006), Advanced insights into sources of vertical velocity in the ocean, *Ocean Dyn.*, doi:10.1007/s10236-005-0050-1.

Hazeleger, W., and S. S. Drijfhout (2000), Eddy subduction in a model of the subtropical gyre, *J. Phys. Oceanogr.*, *30*(4), 677–695, doi:10.1175/1520-0485.

Henning, C. C., and G. K. Vallis (2005), The effects of mesoscale eddies on the stratification and transport of an ocean with a circumpolar channel, *J. Phys. Oceanogr.*, *35*, 880–896.

Lapeyre, G., P. Klein, and B. L. Hua (2006), Oceanic restratification forced by surface frontogenesis, *J. Phys. Oceanogr.*, *36*(8), 1577–1590.

Lavender, K. L., R. E. Davis, and W. B. Owens (2002), Observations of open-ocean deep convection in the Labrador Sea from subsurface floats, *J. Phys. Oceanogr.*, *32*(2), 511–526, doi:10.1175/1520-0485(2002)032.

Le Cann, B., M. Assenbaum, J.-C. Gascard, and G. Reverdin (2005), Observed mean and mesoscale upper ocean circulation in the midlatitude northeast Atlantic, *J. Geophys. Res.*, *110*, C07S05, doi:10.1029/2004JC002768.

Legal, C., et al. (2007), Diagnosis of the vertical pump in a mesoscale stirring region, *J. Phys. Oceanogr.*, in press.

Lévy, M., L. Mémery, and G. Madec (1998), The onset of a bloom after deep winter convection in the North Western Mediterranean sea: Mesoscale process study with a primitive equation model, *J. Mar. Res.*, *16*, 7–21.

Lévy, M., M. Gavart, L. Mémery, G. Caniaux, and A. Paci (2005), A four-dimensional mesoscale map of the spring bloom in the northeast Atlantic (POMME experiment): Results of a prognostic model, *J. Geophys. Res.*, *110*, C07S21, doi:10.1029/2004JC002588.

Lherminier, P., J.-C. Gascard, and D. Quadfasel (1999), The Greenland Sea in water 1993 and 1994: Preconditioning for deep convection, *Deep Sea Res. Part II*, *46*(6–7), 1199–1235, doi:10.1016/S0967-0645(99)00020-X.

Lherminier, P., R. R. Harcourt, R. W. Garwood, and J.-C. Gascard (2001), Interpretation of mean vertical velocity measured by isobaric floats during deep convective events, *J. Mar. Sys.*, *29*(1–4), 221–237, doi:10.1016/S0924-7963(01)00018-5.

Madec, G., P. Delecluse, M. Imbard, and C. Lévy (1999), Opa 8.1 ocean general circulation model reference manual, *Tech. rep.*, Institut Pierre-Simon Lalace (IPSL), Paris, France, note du Pôle de Modélisation du Climat No. XX. Available at http://www.ipsl.jussieu.fr.

Marshall, D. (1997), Subduction of water masses in an eddying ocean, *J. Mar. Res.*, *55*, 201–222.

Marshall, J. C., A. J. G. Nurser, and R. G. Williams (1993), Inferring the subduction rate and period over the North Atlantic, *J. Phys. Oceanogr.*, *23*, 1315–1329.

Mémery, L., G. Reverdin, J. Paillet, and A. Oschlies (2005), Introduction to the POMME special section: Thermocline ventilation and biogeochemical tracer distribution in the northeast Atlantic Ocean and impact of mesoscale dynamics, *J. Geophys. Res.*, *110*, C07S01, doi:10.1029/2005JC002976.

Nurser, A. J. G., and J. W. Zhang (2000), Eddy-induced mixed layer shallowing and mixed layer/thermocline exchange, *J. Geophys. Res.*, *105*(C9), 21,851–21,868.

Oschlies, A. (2002), Improved representation of upper-ocean dynamics and mixed layer depths in a model of the North Atlantic on switching from eddy-permitting to eddy-resolving grid resolution, *J. Phys. Oceanogr.*, *32*(8), 2277–2298, doi:10.1175/1520-0485(2002)032.

Paci, A., G. Caniaux, M. Gavart, H. Giordani, M. Lévy, L. Prieur, and G. Reverdin (2005), A high resolution simulation of the ocean during the POMME experiment: Simulation results and comparison with observations, *J. Geophys. Res.*, *110*, C07S09, doi:10.1029/2004JC002712.

Paillet, J. (1999), Central water vortices of the eastern North Atlantic, *J. Phys. Oceanogr.*, *29*(10), 2487–2503, doi:10.1175/1520-0485.

Paillet, J., and M. Arhan (1996a), Shallow pycnoclines and mode water subduction in the eastern North Atlantic, *J. Phys. Oceanogr.*, *26*, 96–114.

Paillet, J., and M. Arhan (1996b), Oceanic ventilation in the eastern North Atlantic, *J. Phys. Oceanogr.*, *26*, 2036–2052.

Qiu, B., and R. X. Huang (1995), Ventilation of the North Atlantic and North Pacific: Subduction vs. obduction, *J. Phys. Oceanogr.*, *25*, 2374–2390.

Qu, T., S.-P. Xie, H. Mitsudera, and A. Ishida (2002), Subduction of the North Pacific mode waters in a global high-resolution GCM, *J. Phys. Oceanogr.*, *32*(3), 746–763, doi:10.1175/1520-0485(2002)032.

Reverdin, G., M. Assenbaum, and L. Prieur (2005), Eastern North Atlantic mode waters during POMME (September 2000–2001), *J. Geophys. Res.*, *110*, C07S04, doi:10.1029/2004JC002613.

Steffen, E. L., and E. A. D'Asaro (2002), Deep convection in the Labrador Sea as observed by Lagrangian floats, *J. Phys. Oceanogr.*, *32*(2), 475–492, doi:10.1175/1520-0485(2002)032.

Stevenson, J. W., and P. P. Niiler (1983), Upper ocean heat budget during the Hawaii-to-Tahiti Shuttle Experiment, *J. Phys. Oceanogr.*, *13*(10), 1894–1907, doi:10.1175/1520-0485(1983)013.

Takahashi, T., T. T. Takahashi, and S. C. Sutherland (1995), An assessment of the role of the North Atlantic as a CO_2 sink, *Philos. Trans. R. Soc. London, Ser. B*, *348*, 143–152.

Thiele, G., and J. L. Sarmiento (1990), Tracer dating and ocean ventilation, *J. Geophys. Res.*, *95*, 9377–9391.

Tsujino, H., and T. Yasuda (2004), Formation and circulation of mode waters of the north Pacific in a high-resolution GCM, *J. Phys. Oceanogr.*, *34*(2), 399–415, doi:10.1175/1520-0485.

Valdivieso Da Costa, M., H. Mercier, and A.-M. Tréguier (2005), Effect of the mixed-layer time variability on kinematic subduction rate diagnostics, *J. Phys. Oceanogr.*, *35*(4), 427–443, doi:10.1175/JPO2693.1.

van Aken, H. (2001), The hydrography of the mid-latitude northeast Atlantic Ocean. part III: The subducted thermocline water masses, *Deep Sea Res. Part I*, *48*, 237–267.

Weller, R. A., P. W. Furey, M. A. Spall, and R. E. Davis (2004), The large-scale context for oceanic subduction in the northeast Atlantic, *Deep Sea Res. Part I*, *51*, 665–699.

Williams, R. G., M. A. Spall, and J. C. Marshall (1995), Does Stommel's mixed layer 'demon' work?, *J. Phys. Oceanogr.*, *25*, 3089–3102.

G. Caniaux, H. Giordani, and A. Paci, Centre National de Recherches Météorologiques-Groupe d'Etude de l'Atmosphère Météorologique, URA 1357 Météo-France/CNRS, 42 av. G. Coriolis, 31057 Toulouse Cedex 01, France. (alexandre.paci@meteo.fr)

M. Lévy and G. Reverdin, LOCEAN/IPSL, University of Paris VI, BP100, 4 place Jussieu, 75252 Paris Cedex 05, France.

L. Prieur, LOV, BP 28, 06234 Villefranche-sur-Mer Cedex, France.